

Experimental and numerical study of a lightweight steel-concrete bridge deck concept

*Peter Helincks¹⁾, Wouter De Corte²⁾, Veerle Boel³⁾ and Geert De Schutter⁴⁾

1), 2), 3) Department of Industrial Technology & Construction, Faculty of Engineering and Architecture, Ghent University, Valentin Vaerwyckweg 1, B-9000 Ghent, Belgium

1), 2), 3), 4) Magnel Laboratory for Concrete Research, Department of Structural Engineering, Ghent University, Technologiepark 904, B-9052 Zwijnaarde, Belgium

¹⁾ peter.helincks@hogent.be, ²⁾ wouter.decorte@hogent.be

ABSTRACT

In this paper, a lightweight steel-concrete deck concept is presented, combining the advantages of both concrete and steel deck types and avoiding their disadvantages. In this concept, a network of longitudinal and transverse ribs transmit shear forces between thin steel top and bottom plates. In order to achieve a lightweight composite structure, the concrete volume is only 32 % of the volume between the plates. The first part of the paper describes static loading tests on a full scale bridge deck test panel (3.60 m x 1.50 m). First, the general behaviour is examined by applying a 100 kN wheelload on multiple positions thereby determining the amount of transverse load spreading. Second, the most adverse position is chosen for a static ultimate failure load test at 960 kN. Third, also the local behaviour, i.e. the transverse bending in the top plate and the ribs, due to direct load introduction is tested in failure due to shear for a 600 kN wheelload. In the second part, a finite element model of the test panel is created and verified with the experimental data set of the 100 kN static loading tests. Afterwards, a numerical study is carried out with this finite element model to optimize the bridge deck characteristics, such as rib thickness, rib spacing, and plate thicknesses. The results indicate that the lightweight steel-concrete sandwich bridge deck concept possesses the necessary static resistance to bridge loads.

1. INTRODUCTION

In this research, a new type of bridge deck panel is studied in detail. This component carries the traffic load and is borne by the mean load carrying structure of the bridge, to which the deck is usually connected in order to obtain structural cooperation. In general, it is made of concrete and/or steel, but also fiber-reinforced polymer decks are already applied in small (pedestrian) bridges (Lombardi 2011).

Concrete bridge decks (Fig. 1a, Reid 2012) are constructed with reinforced or prestressed concrete and have typically a thickness of 20 to 30 cm. The connection with the supporting structure is realized by steel stirrups, when the main girders are

Note: Copied from the manuscript submitted to "Steel and Composite Structures, An International Journal" for presentation at ASEM13 Congress

made out of concrete, or welded shear connectors, if steel girders are used (Chen 2000). This form of construction has the clear advantage of having a low cost price.

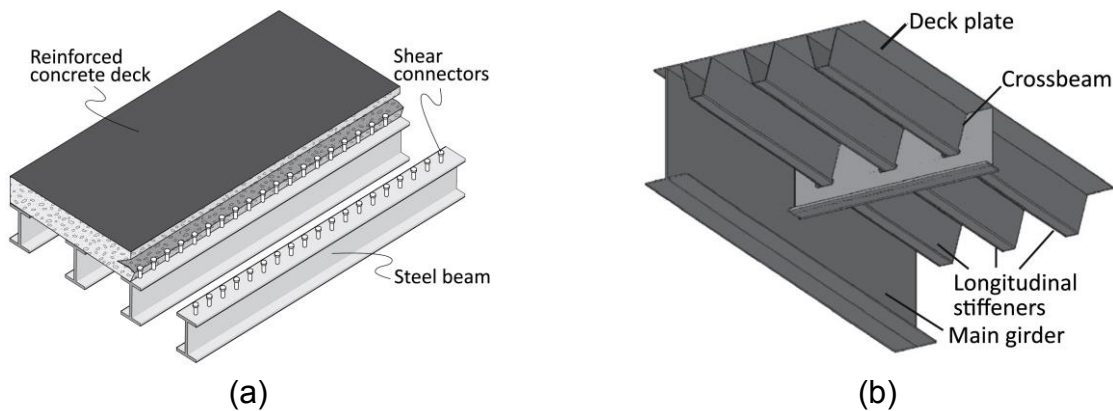


Fig. 1 (a) Concrete deck and (b) steel orthotropic deck

On the other hand, it also has two major shortcomings: the dead weight is substantial, due to the ponderous structure and the concrete deck slab is exposed to weather influences and de-icing salts (Cusson 2010).

Welded steel decks are often employed since their introduction in the 1960's. They consist of a thin steel deck plate (12-18 mm), which is stiffened in two mutually perpendicular directions by means of welded longitudinal stiffeners and crossbeams (Fig. 1b, Teixeira 2010). Since the stiffening is not the same for both directions, this bridge deck is called orthogonal-anisotropic, or, briefly, orthotropic (Connor 2012). The main advantage of the steel orthotropic bridge deck is the light weight, due to the slender elements. By replacing existing reinforced concrete decks with orthotropic deck systems in long-span bridges in Canada and the United States, reductions between 18 and 25 % were achieved. As a result of this decrease, the stresses in the cables and towers of suspension bridges could be reduced with 60-70 % (Chen 2000). However, also these orthotropic bridge decks show some disadvantages. In comparison with concrete decks, the cost price increases with about 300 %, due to the large amount of elements, that need to be welded. Furthermore, these welds lead to a second major drawback of this bridge deck concept: a reduced fatigue resistance (Sim 2009, Nguyen 2011). A limited efficiency of the system is observed because of fatigue phenomena in the welding joints between deck and stiffeners on the one hand and longitudinal stiffeners and crossbeams on the other hand (De Corte 2005a). In addition, the anisotropic nature of the orthotropic deck encourages the fatigue problems, as the applied traffic loads are not uniformly distributed, neither in transverse direction, nor between longitudinal and transverse direction (De Corte 2005b).

In this paper, a new bridge deck concept is proposed, eliminating the above mentioned disadvantages in the largest manner. The prototype deck composition consists of a concrete sandwich core (Fig. 2a) between two thin steel plates at the bottom and top position. The connection between both materials is realized with a two-component epoxy adhesive layer. The space between the outer plates is filled with unreinforced high self-compacting concrete, be it with a large void ratio, realized by

polystyrene blocks. The concrete generates a 2D grid structure between the outer plates, creating both a shear connection as well as virtual supports for the top plate. In this last action, the concrete ribs limit the transverse bending stresses in the top plate when a concentrated wheel load is situated between these ribs. However, compared to the corresponding action in an orthotropic deck, no welds are present in the top plate. Consequently, the allowable fatigue cycle can be twice as higher, allowing a plate thickness reduction of 30 to 40%. The isotropic behaviour is realized by 2 or 3 transverse concrete ribs in between the traditional floorbeams spaced 4 to 5 m apart. A reduction of the rib distortion effect, combined with the additional transverse stiffness realizes a more isotropic effect. This reduces longitudinal bending moments generated by the concentrated wheel loads. Given the narrow rib dimensions and the presence of transverse ribs, the use of high strength fiber reinforced self-compacting concrete is required. This concrete is specifically designed not to require external energy for compaction.

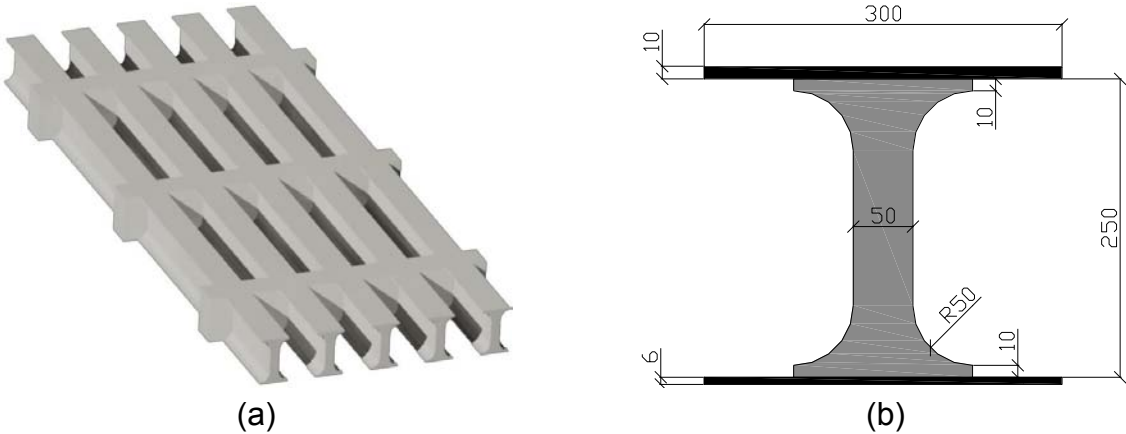


Fig. 2 (a) Concrete network of deck panel and (b) dimensions of longitudinal ribs [mm]

In the first part of this paper, the structural static behaviour of the sandwich deck concept is investigated. First, the general behaviour is examined by applying a 100 kN wheelload on multiple positions thereby determining the amount of transverse load spreading. Second, the most adverse position is chosen for a static ultimate failure load test at 960 kN. Third, also the local behaviour, i.e. the transverse bending in the top plate and the ribs, due to direct load introduction is tested with failure due to shear for a 600 kN wheelload. In the second part, a finite element model of the test panel is created and verified with the experimental data set of the 100 kN static loading tests. Afterwards, a numerical study is carried out with this finite element model to optimize the bridge deck characteristics, such as rib thickness, rib spacing, and plate thickness.

2. EXPERIMENTAL RESEARCH

An experimental test program was carried out to examine the structural performance of the proposed sandwich deck. Both the general and local behaviour were studied by executing various static loading tests on 3.6 m x 1.5 m sandwich deck test panels. In

addition, also the ultimate bearing capacity of one of the decks was determined for the most adverse load situation based on the non-destructive 100 kN loading tests.

2.1 Sandwich deck test panels – Geometry and materials

Two experimental test panels were fabricated with a length of 3.60 m and a width of 1.50 m. For each deck panel, five longitudinal and three transverse concrete ribs were vertically cast between the steel plates, with a rib spacing of 0.30 m and 1.20 m, respectively (Fig. 2a). The dimensions of the longitudinal ribs are given in Fig. 2b. The transverse concrete ribs had a rectangular shape with a height of 250 mm and a width of 150 mm. At the top and the bottom of the sandwich panels, thin steel plates (3.6 m x 1.5 m) were provided, with thicknesses of 10 and 6 mm.

Concrete mixture As already mentioned above, the main function of the concrete ribs is to transfer the shear forces between top and bottom steel plate. Since the rib dimensions are rather limited, the use of a high-performance fiber-reinforced self-compacting concrete is essential. In this research, the concrete premix REFOR-tec® GF5 ST-HS produced by Tecnochem Italiana S.p.A. was applied. This micro-concrete consists of three components: a powder, a liquid, and a fiber component, mixed with a mass ratio of 1000:115:45. The composition and/or characteristics of these components are summarized in Table 1. In addition, the main characteristics of this concrete mixture according to EN 1504-3, as reported Tecnochem (2010), are listed in Table 2. During casting, an average slump flow of 715 mm was measured according to EFNARC (2005). Together with the deck panels, cylindrical (diameter 150 mm and height 300 mm) and cubic (side 150 mm) test samples were also cast in order to determine the compressive strength at testing age. These specimens were demoulded after 1 day and sealed and stored next to the bridge deck elements.

Table 1 Composition of concrete premix REFOR-tec® GF5 ST-HS

Powder	Liquid	Fibers
CEM I 52.5	Water (w/c-ratio of 0.30)	Steel fibers
CEM II/A-S 52.5	Polycarboxylate	FIB-energy® ST/HS
Micro-silica based powder	superplasticizer	Diameter 200 µm
MICROBETON POZ	Defoamer	Length 15 mm
Micro-silica based powder	Shrinkage reducing agent	Tensile strength
MICROBETON POZ/H		> 2 800 N/mm ²
Polycarboxylate		Modulus of elasticity
superplasticizer		210 000 N/mm ²
TECNOS® 100 azur WPT		
Polyvinyl alcohol fibers		
FIB-energy® MC 40/8		

Steel plates For the top and bottom plate, hot-rolled construction steel S235 according to EN 10025-2 was used, with a guaranteed minimum yield strength of 235 N/mm². In

order to obtain improved bonding conditions, both steel plates were steel grit blasted, resulting in a rough surface.

Steel-concrete interlayer For the adhesive layer, a two-component epoxy resin

Table 2 Properties of concrete premix REFOR-tec[®] GF5 ST-HS

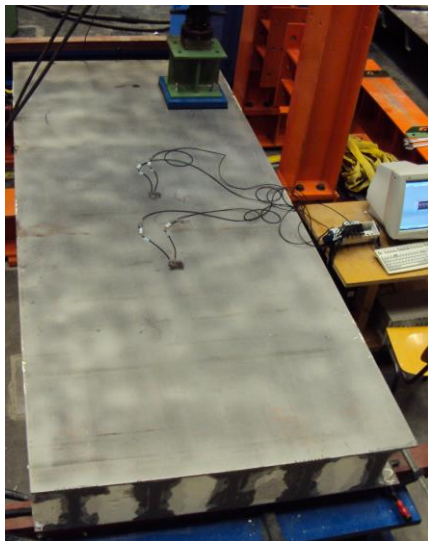
Properties*	
Workability time	> 1h
Density	2450 kg/m ³
Compressive strength at 28 days	130 N/mm ²
Tensile strength at 28 days	8.8 N/mm ²
Flexural strength at 28 days	32 N/mm ²
Modulus of elasticity	38000 N/mm ²

* Values obtained with liquid demand 11 % on samples 4x4x16 cm (according to UNI EN 1504-3)

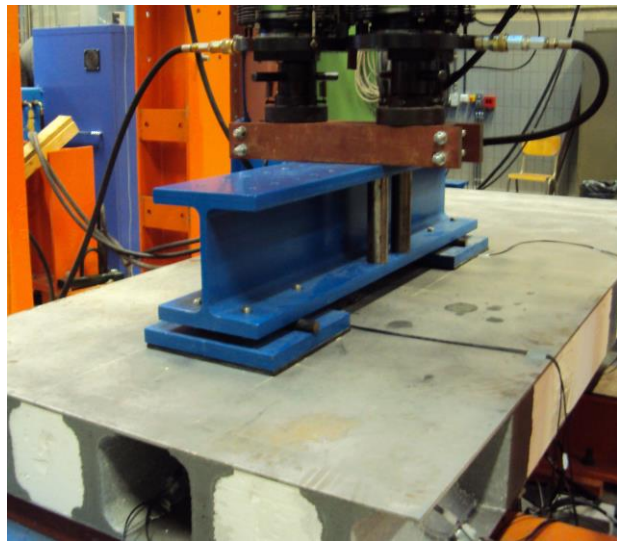
Tecnoepo 400 (Tecnochem 2007) with very high adhesion to e.g. cement based substrates and steel was used. Due to its high fluidity, the epoxy was applied on the steel plates with a paint roller, resulting in a layer thickness between 1 and 2 mm. Additionally, the fresh epoxy adhesive layer was gritted with steel grit (0.2/1.5) before hardening to enhance the bond strength. For these bonding conditions, an average shear bond stress of 4.65 N/mm² was found in Helincks (2013).

2.2 Test setup

General static loading tests For both the 100 kN non-destructive loading tests and the ultimate failure load test, an identical test setup was used (Fig. 3). The composite deck element was placed on two neoprene supports (width 20 mm) with a span of 3.40 m. For the 100 kN load tests, the force was applied with a 600 kN jack on a square surface of 400 x 400 mm, according to Load Model 1 (LM1) from EN 1991-2. In order to achieve a proper distribution of the load, the 100 kN force was applied on a steel profile, placed on a square neoprene rubber with side 400 mm and a thickness of 15 mm. To study the structural behaviour, the load was placed on multiple locations as shown in



(a)



(b)

Fig. 3 (a) 100 kN loading test and (b) ultimate failure load test setup

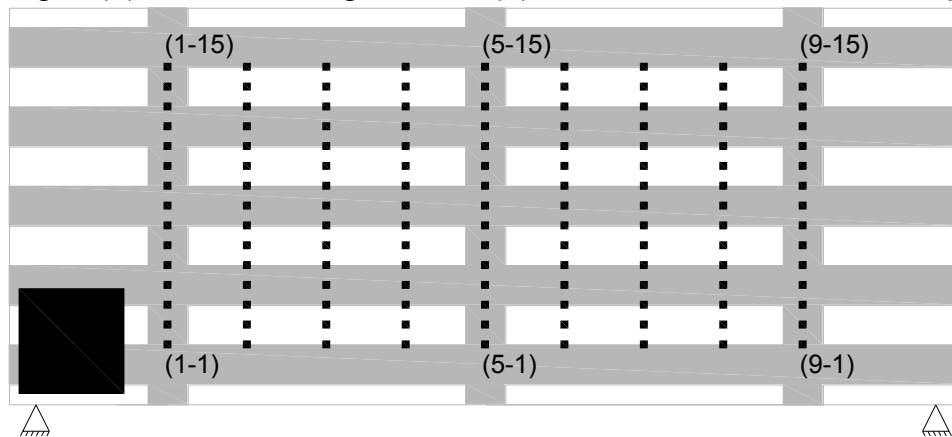


Fig. 4 Load surface and load positions for the 100 kN static loading tests

Fig. 4. Additionally, the shape of the load surface and the name of all load locations are also given in this image. This test was carried out on both deck test panels.

In order to determine the ultimate failure load of one of the sandwich panels, two 600 kN jacks were used. Here, the load was applied on two square surfaces with a side of 400 mm and a distance of 1.20 m between the load centres by using a steel load spreader, a HE300M steel profile. This setup corresponds with the wheelload configuration of LM1. The two load surfaces were located on load positions (1-8) and (5-8), as illustrated in Fig. 4. Also here, the load was applied on a neoprene rubber to achieve a good load introduction in the bridge deck panel.

During these two tests, various steel and concrete strains were recorded. In total, 31 strains values were measured using 23 strain gauges (LY41-10) on the bottom steel plate (S1-S23), 2 strain gauges of the rosette type (TML-PC-10) on the upper steel

plate (ST1 and ST2, with L=longitudinal and T=transverse), and 4 strain gauges (PL-60-11) on the concrete ribs (C1-C4). The positions and names of all strain gauges are given in Fig. 5.

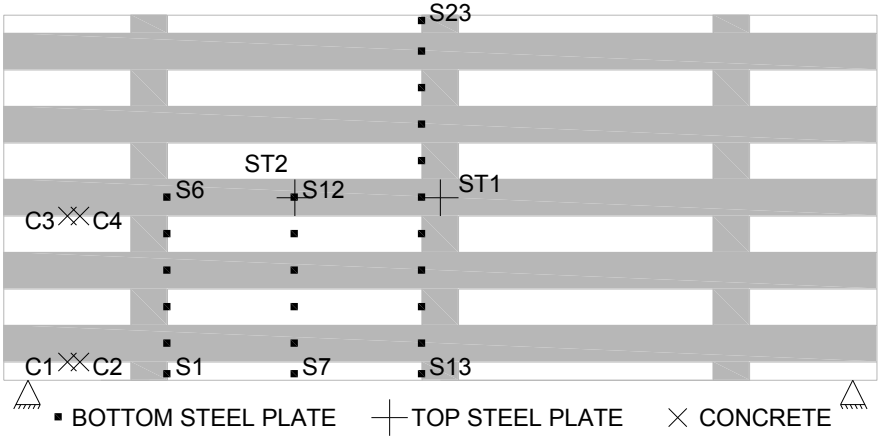


Fig. 5 Name and position of steel and concrete strain gauges

Local bending tests For the local bending tests, the undamaged part of the deck panel (right side on Fig. 5) was fully supported in transverse direction, as illustrated in Fig. 6. For the first test, the most concentrated load according to EN 1991-2 was chosen, wheelload C in particular (60 kN on a surface of 320 mm x 270 mm). For this test, the force was applied on load position 1 (see Fig. 6) and steel (S1) and concrete strains (C1-C3) were continuously recorded using 4 strain gauges, of which the locations are also depicted in Fig. 6. Afterwards, two local bending tests up to failure were performed: one test on load position 1 up to 600 kN with continuous strain monitoring and one test on load position 2 up to 500 kN without strain measurements.

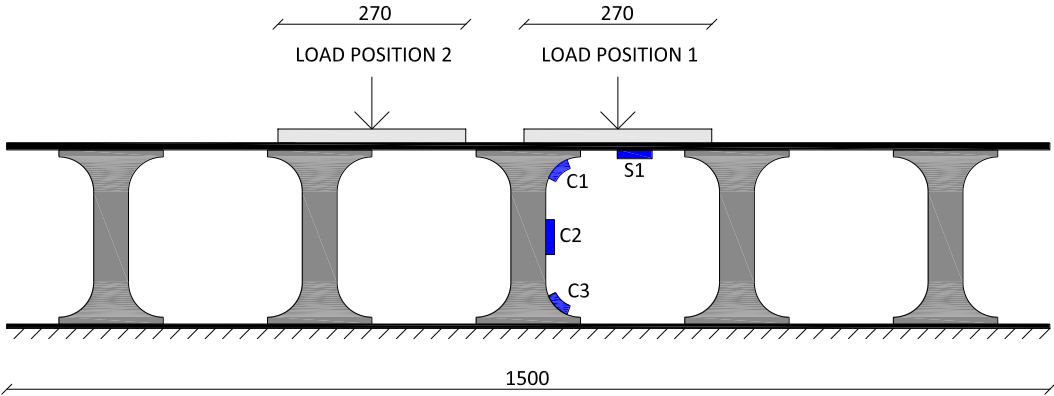


Fig. 6 Local bending test setup and location of strain gauges

2.3 Results and discussion

100 kN loading tests For deck 1 and deck 2, the 100 kN static load tests were started at an age of 152 and 128 days, respectively. The compressive strength of the concrete, used to cast the bridge deck test panels, was determined on the first testing day. The

results for both cylindrical and cube compressive strength (f_{cm} and $f_{c,cubm}$) according to NBN EN 12390-3 and standard deviations are listed in Table 3.

Table 3 Cylindrical and cube compressive strength at testing age

	Deck 1 (152 days)	Deck 2 (128 days)
f_{cm} [N/mm ²]	98.7 (7 samples)	92.5 (5 samples)
stdev	10.8	8.1
$f_{c,cubm}$ [N/mm ²]	101.7 (6 samples)	95.3 (4 samples)
stdev	10.5	7.4

The steel stresses in the bottom steel plate on locations S1-S6 show a maximum value when the load is applied just above these strain gauges (load position (1-1)), with maximum stresses (S1) of 26.0 and 30.8 N/mm², for deck 1 and deck 2 (Fig. 7) respectively. Also for S7-S12, the largest values are measured when the load is applied above these strain gauges, and in particular on position (3-1), which are pictured in Fig. 8 for deck 2. For deck 1 and 2, the maximum stress occurs in S7, equal to 41.2 N/mm² (deck 1) and 45.4 N/mm² (deck 2). For the other strain gauges on the bottom steel plate (S13-S23), the largest strain values are recorded when the load is applied in the middle of the deck panel, on load positions (5-1) to (5-15) in particular. The maximum stresses are found for S14 (deck 1) and S22 (deck 2) and are equal to 29.6 and 31.8 N/mm². For deck 2, the relevant stresses are depicted in Fig. 9.

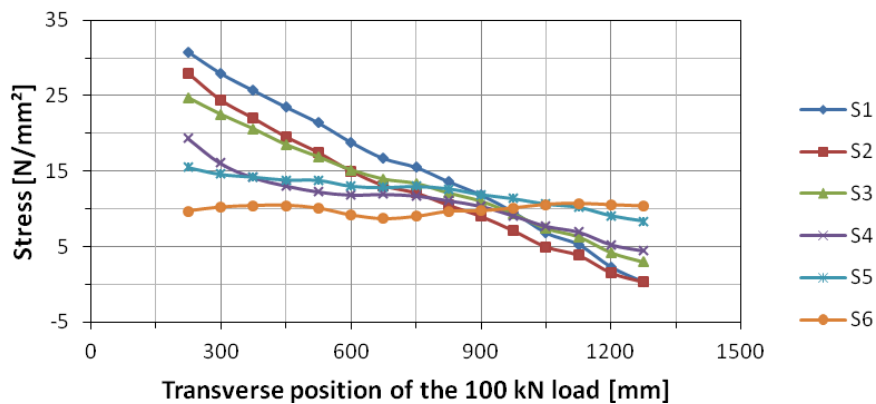


Fig. 7 Steel stresses (S1-S6) for load positions (1-1) to (1-15) (deck 2)

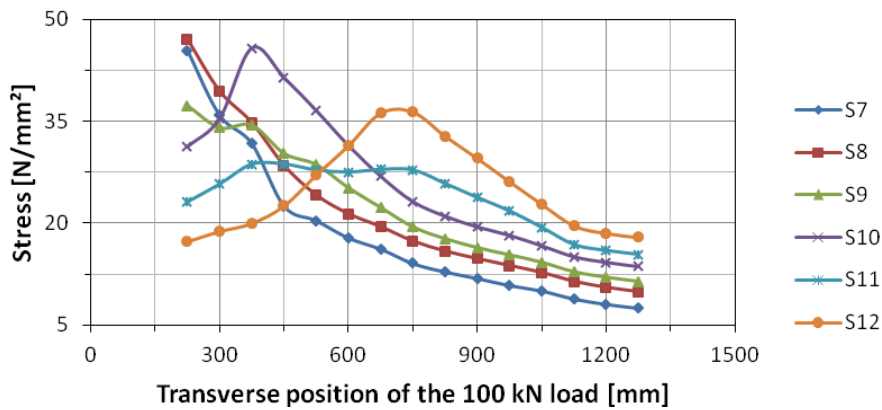


Fig. 8 Steel stresses (S7-S12) for load positions (3-1) to (3-15) (deck 2)

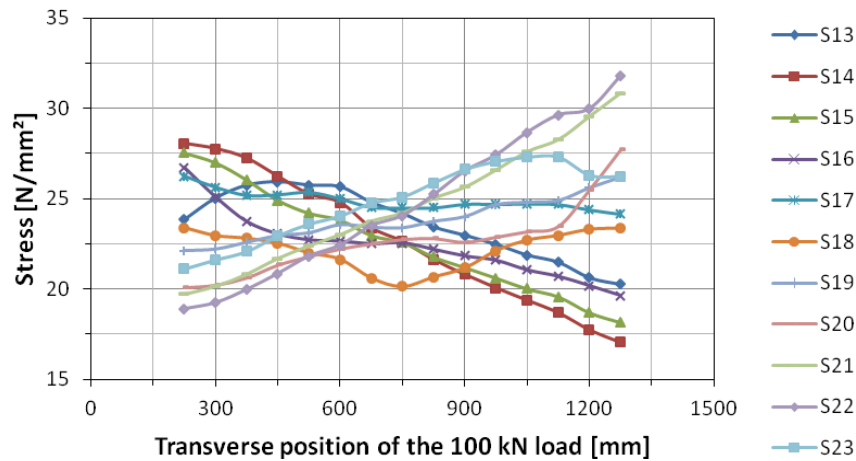


Fig. 9 Steel stresses (S13-S23) for load positions (5-1) to (5-15) (deck 2)

When the experimental data sets of deck 1 and deck 2 are compared, a stress ratio between 0.71 and 1.45 is found, with an average value of 0.94. Thus, it can be concluded that, a rather good accordance between the behaviour of the two bridge deck test panels is observed based on the steel stresses S1-S23.

The similar static behaviour of the two bridge deck panels is clearly visible in Fig. 10 and Fig. 11, where the stresses of both decks are summarized in the same chart. Fig. 10 shows the compressive stresses, occurring in the top steel plate, for load positions (3-1) to (3-15), where the maximum compressive stress of 36.3 N/mm² for deck 2 is found. Here, the average stress ratio is also 0.94. The concrete tensile and compressive stresses of both decks are shown in Fig. 11. Also here, the good accordance between the two experimental measurements is noticed (mean value of the stress ratio of 0.92). Since the concrete strain gauges are applied on the concrete ribs close to the support, the largest strain values are obtained for load positions (1-1) to (1-15). The maximum tensile and compressive stress are both found for load position (1-1) and have a magnitude of 4.34 N/mm² (C1 of deck 1) and 3.93 N/mm² (C2 of deck 2).

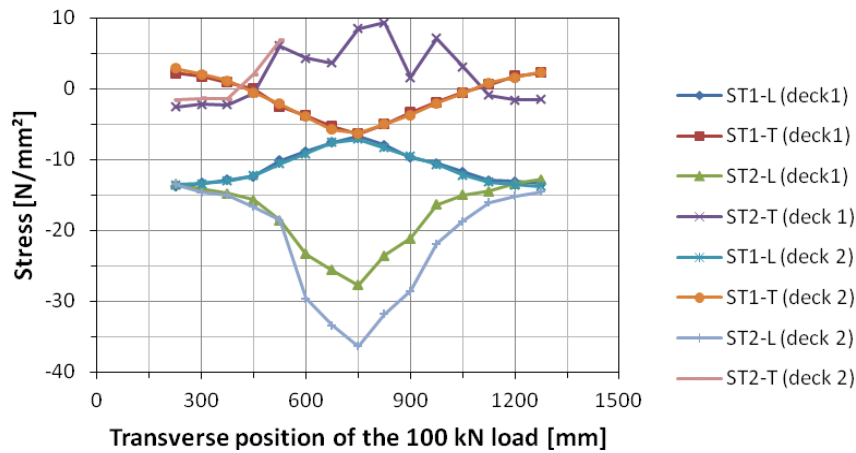


Fig. 10 Steel stresses (ST1 and ST2) for load positions (3-1) to (3-15)

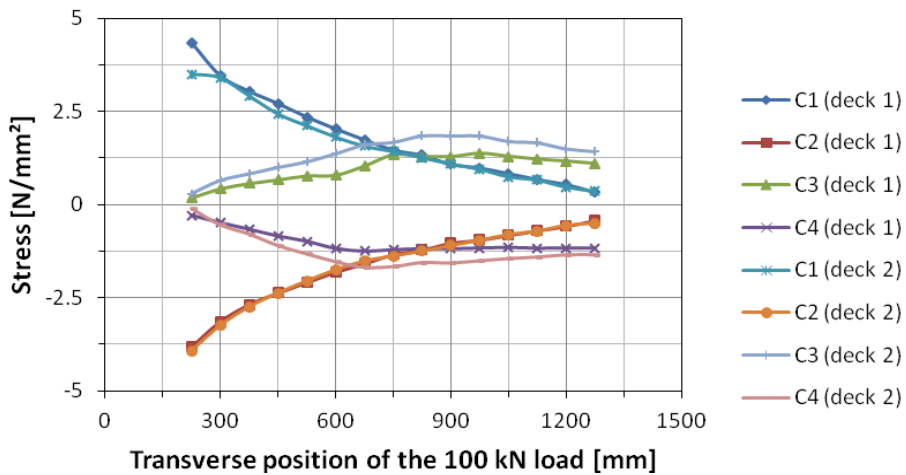


Fig. 11 Concrete stresses for load positions (3-1) to (3-15)

In order to evaluate to what extent the bridge deck concept is able to spread the applied wheelload transversely, the longitudinal steel stresses, corresponding with the strains measured on the bottom steel plate of deck 1, are plotted in Fig. 12 for two load positions where the wheelload is located above the middle longitudinal concrete rib, namely load position (3-8), where the load is applied between the transverse ribs and position (5-8), where it is positioned above the transverse stiffener in the centre of the bridge deck test panel.

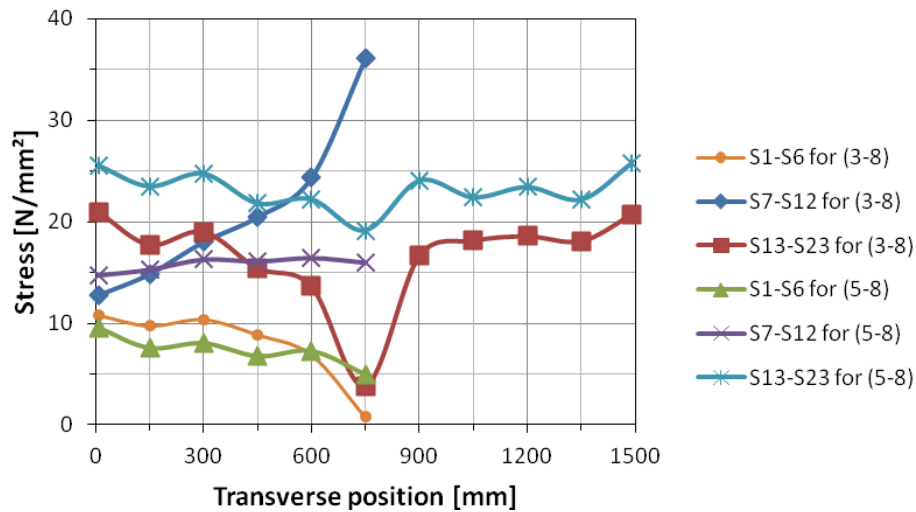


Fig. 12 Transverse load spreading for load positions (3-8) and (5-8)

When the load is applied between the transverse ribs, it can be seen that the central rib is the most loaded (S7-S12 for (3-8)). Despite this fact, a rather good transverse load distribution is found, as the longitudinal steel stresses, determined below the first (S8) and second (S10) rib, are still 41.2 and 56.7 % of the maximum stress in the centre of the deck (S12), equal to 36.12 N/mm². At the intersections with the transverse ribs, the longitudinal stresses show already an improved transverse distribution across the bottom steel plate (S1-S6 for (3-8) and S13-S23 for (3-8)). In addition, contrary to what one would intuitively expect, it is observed that at the location of the transverse ribs, the lowest steel stresses are found in the middle of the cross section.

When the wheelload is applied in the centre of the deck, a good transverse load spreading is obtained, due to the presence of the transverse concrete rib. This is illustrated by the measured values from S13-S23, located directly underneath this rib, ranging from 19.13 to 25.77 N/mm² and the longitudinal steel stresses between the transverse stiffeners (S7-S12), situated between 14.75 and 16.46 N/mm². Also here, the longitudinal stress distribution across the bottom steel plate exhibits a minimum in the centre below the transverse ribs.

Ultimate failure load test The load was gradually increased with a speed of about 80 kN per minute until ultimate failure occurred at 960 kN. As expected, the bridge deck panel showed shear failure in all longitudinal concrete ribs close to the supports (Fig. 13). Due to the large deformation near the shear cracks, also debonding between concrete and top and bottom steel plate took place, as can be seen in Fig. 13.

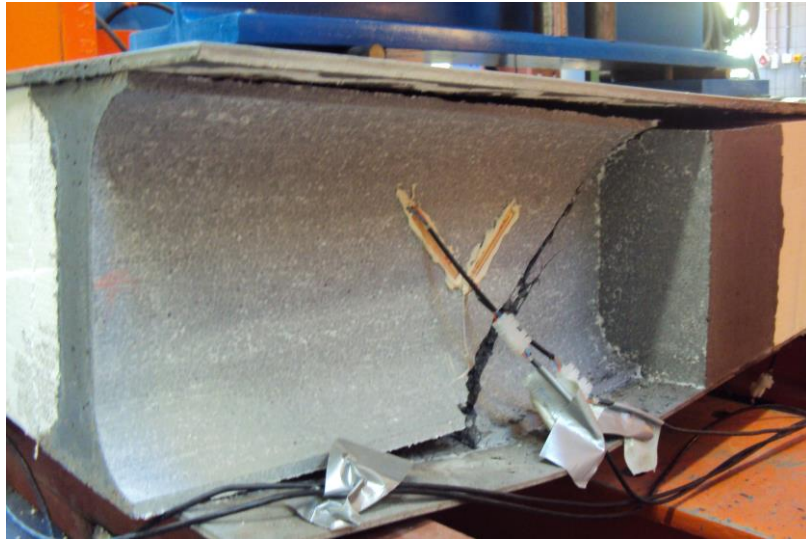


Fig. 13 Ultimate shear failure in static loading test (deck 2)

For this load position, which is the most adverse situation based on the 100 kN static loading tests, the bearing capacity of the bridge deck panel is 960 kN. Taking into account the partial safety factor for concrete γ_C (1.5 according to EN 1992-1-1 and the partial factor for variable road traffic actions γ_Q (1.35 according to EN 1990 – Annex A2), the load capacity in ultimate limit state of the bridge deck is 474 kN, exceeding the design load of LM1 (300 kN) with 58 %. However, it should be noted that during the numerical research, a more adverse load configuration was found, based on the calculated maximum concrete shear stress.

The measurements of all steel (bottom plate) and concrete strain gauges are visualized in Fig. 14 and Fig. 15. From Fig. 14, it is noticed that all load-stress curves, based on the longitudinal strain recordings on the bottom steel plate, show a nearly linear behaviour, indicating that during the test, the yield strength is never exceeded in the measuring points. Indeed a maximum stress of 234 N/mm² is obtained for S22 just before failure, which is practically equal to the minimum guaranteed yield stress, being 235 N/mm².

The compressive and tensile strains, measured on the concrete ribs in the vicinity of the supports, are displayed in Fig. 15. From this figure, it can be concluded that up to a load of about 500 kN, the load-strain curves show a quasi linear-elastic behaviour. For higher loads, the formation of (large) cracks in the concrete ribs cause a deviant behaviour, resulting in increasing concrete strains. It is interesting to note that with increasing load the recorded tensile strain C1 on the outer longitudinal rib becomes larger than the C3-value, measured on the central rib, even though the load is applied above the latter. It stands to reason that this observation is the consequence of the formation of small cracks in the centre rib, resulting in a redistribution of the concrete

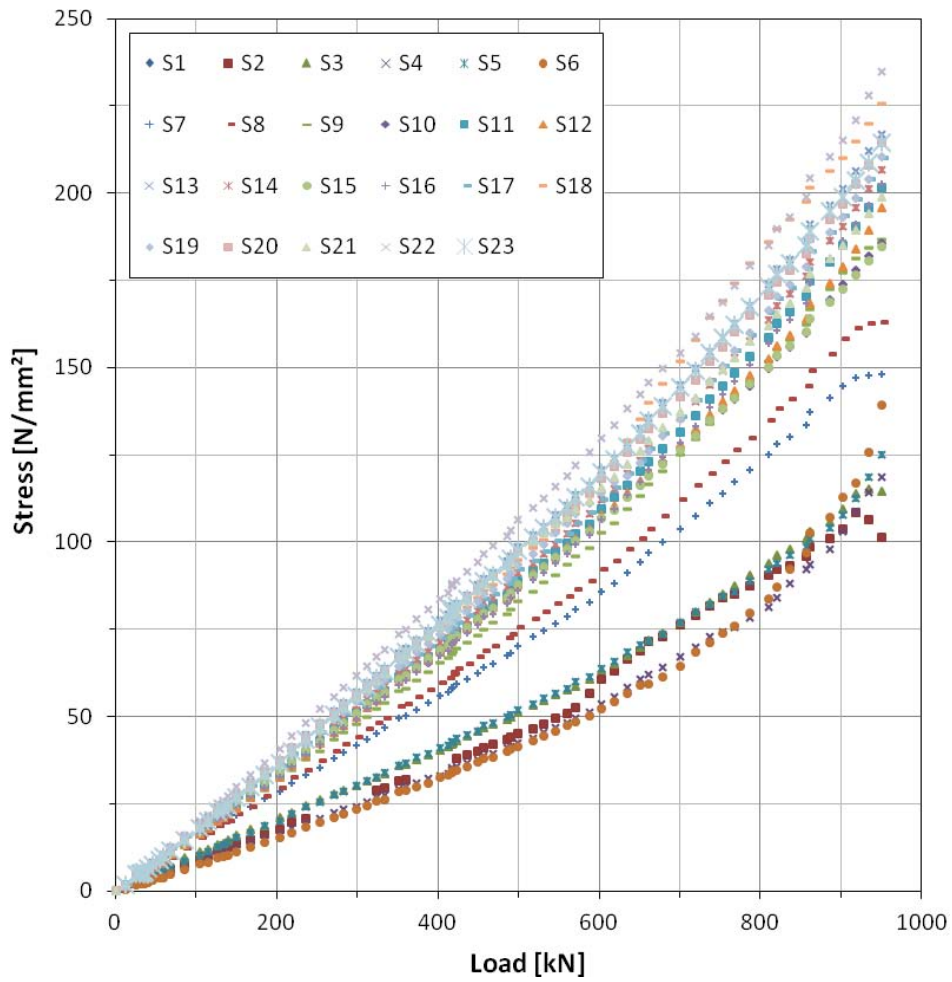


Fig. 14 Steel stresses in bottom steel plate during ultimate failure load test

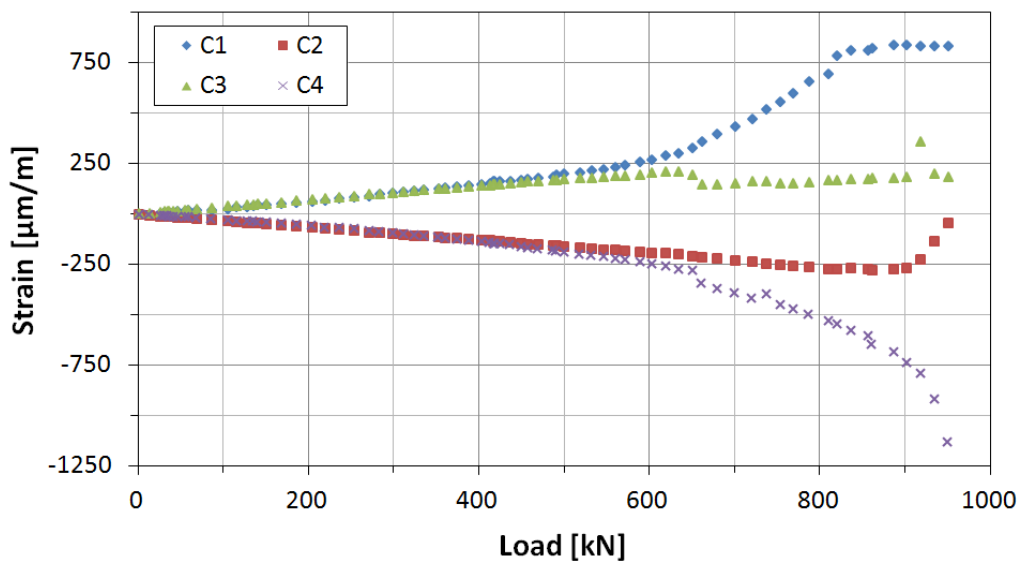


Fig. 15 Concrete strains during ultimate failure load test

stresses, influencing the measured concrete tensile strains locally (C3) and generally (C1). For the compressive strains, it can be seen that the highest values are found on the central rib as expected.

Local bending tests To investigate the local behaviour, first, a 60 kN load was applied on load position 1. The resulting stresses can be seen in Fig. 16. It is noticed that the tensile stress, measured on the bottom side of the top steel plate, remains relatively small for a 60 kN load (38 N/mm²). Also, the occurring concrete compressive stresses are limited to 7.7 N/mm².

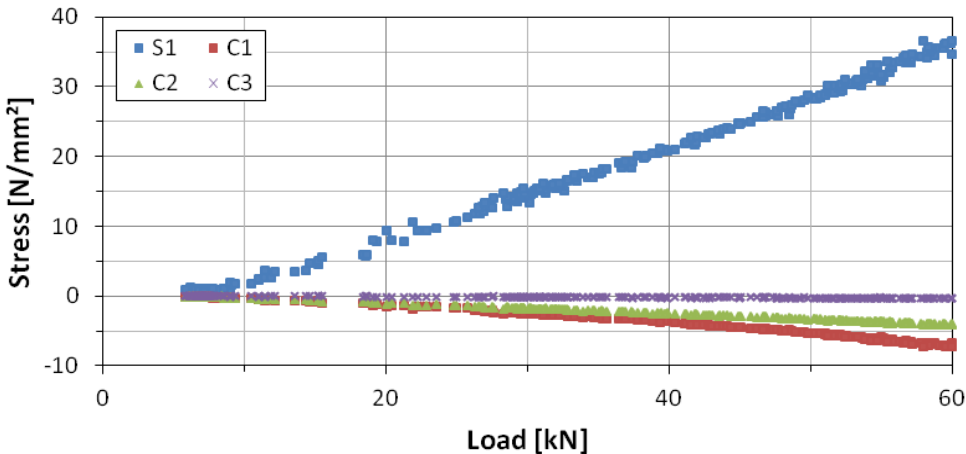


Fig. 16 Stress measurements during first local bending test (60 kN)

During this first local bending test, the load was gradually increased beyond this 60 kN load. At 320 kN, the first crack was heard and became visible in the upper part of the right concrete rib (marked in Fig. 17a). When the load was further increased, it was observed that this crack grew slowly and the upper steel plate showed a large transverse bending. At a load of 600 kN, the test was stopped.



Fig. 17 Concrete rib failure during first (a) and second (b) local bending test

The recorded strain values for S1 and C1-C3 are presented in Fig. 18. With respect to the steel, it is seen that the top steel plate was yielding during the test as a non-linear load-strain curve is noticed. Indeed, the plate showed a small residual deformation

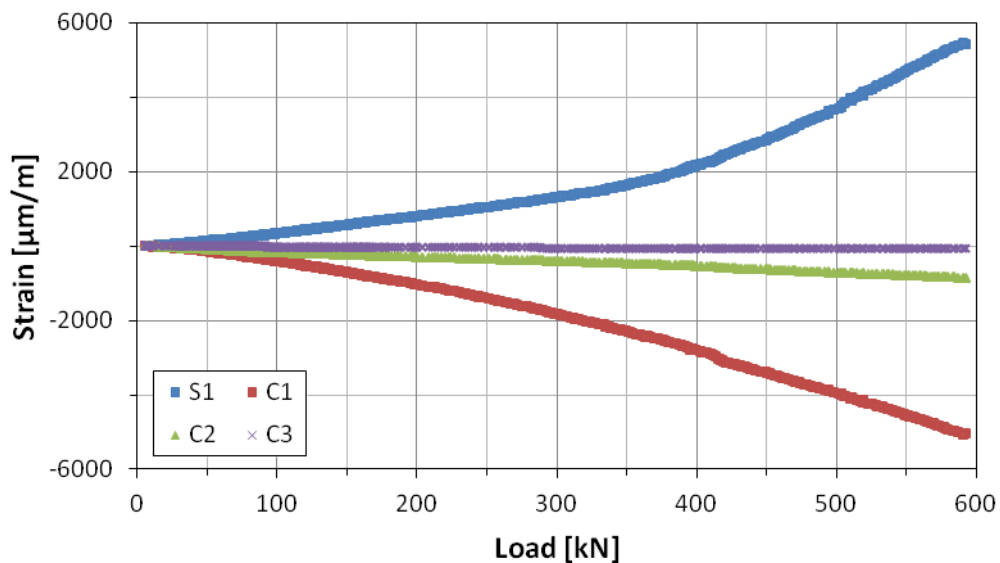


Fig. 18 Strain measurements during first local bending test

between the concrete ribs after the load was removed. The yield stress of 235 N/mm^2 was exceeded for a load of 264 kN . Since no ultimate failure of the concrete rib was observed, the steel stress can be used to determine the bearing capacity in ultimate limit state (ULS). With a partial safety factor for construction steel of 1.1 (EN 1993-2) and a partial factor for variable road traffic actions γ_Q of 1.35 (EN 1990 – Annex A2) the load capacity in ULS for this local verification is 178 kN , which is 2.69 times higher than the design load (60 kN on a wheel surface type C).

For the second local bending test on load position 2, no strains were recorded. Also here, the load was gradually increased up to 600 kN . The first visible crack, marked in Fig. 17b, was seen for a load of about 300 kN . In contrast to the crack in LBT1, this crack was located in the web of the concrete rib, as the load was applied asymmetrically above the rib, resulting in large tensile stresses in the concrete web.

3. NUMERICAL RESEARCH

Next to the experimental tests on the bridge deck test panels, also a numerical study was performed. First, the characteristics of the finite element model (FEM) are discussed, after which the most adverse load position is determined and a parametric study is carried out to optimize the dimensions of the bridge deck elements.

3.1 Finite element bridge deck model

In the finite element software Abaqus, a FEM of the bridge deck test panel was created (Fig. 19). The connection between the steel plates and the concrete ribs was modelled as a tied connection, in order to avoid loss of bond. Two 20 mm wide rigid supports, which are able to rotate around the z-axis, were used to support the bottom steel plate. The materials were characterized by the Young's modulus E and the ratio of

Poisson ν : $E_s=210000 \text{ N/mm}^2$ and $\nu=0.3$ for steel and $E_c=38000 \text{ N/mm}^2$ and $\nu=0.2$ for concrete. The steel plates were meshed using 8-node linear brick elements (C3D8). For the top and bottom steel plate, a mesh seed of 10 and 5 mm was chosen. For the concrete rib network, 4-node linear tetrahedrons (C3D4) were used with a mesh seed of 30 mm. Only for the end parts of the longitudinal ribs, where the strain gauges were positioned, a smaller mesh seed was applied (15 mm) (see Fig. 20).

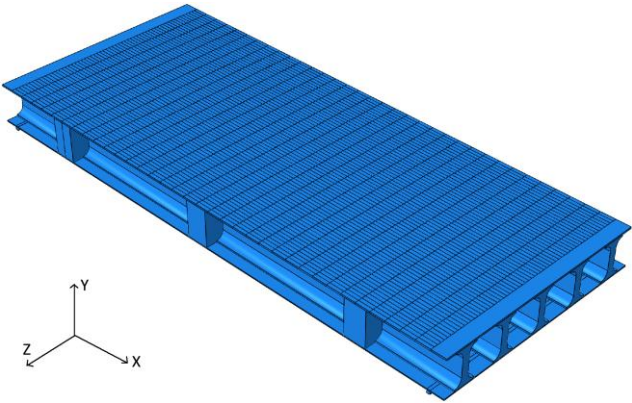


Fig. 19 Finite element model of the bridge deck test panel

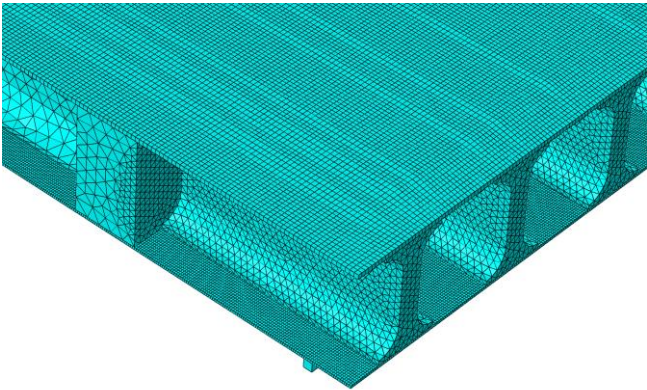


Fig. 20 Meshed bridge deck model

The FEM was verified with the experimental data sets of the 100 kN loading tests. Both the numerical results, determined at the exact strain gauge locations, and experimental results for S1-S23 are visualized in Fig. 21 for load position (5-8). Based on this graphic representations, it is clear that a good agreement between numerical and experimental results is found, with a mean ratio between numerical and experimental stresses of 1.04 is calculated, with a minimum and maximum of 0.93 and 1.17. Also for the other strain gauges, the numerical stresses are in good accordance with the experimental measurements. For load position (5-8) in particular, the numerical steel stresses in the upper steel plate are on average 94.0 % of the corresponding mean experimental values. For the concrete strain gauges, mean ratios of 0.89 and 1.07 are found, for deck 1 and deck 2 respectively. Based on the comparison between numerical and experimental results for all strain gauges, it can be concluded that the

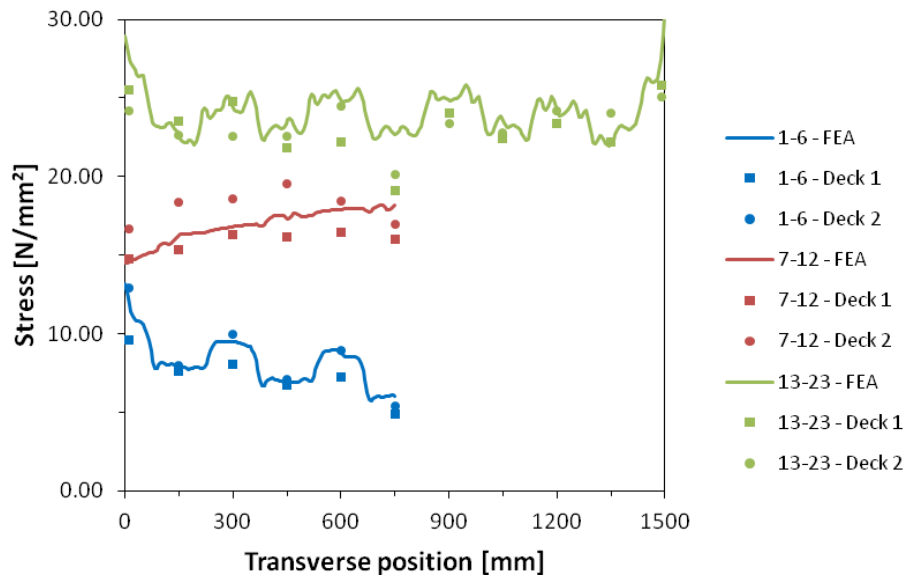


Fig. 21 Experimental and numerical stress results (S1-S23) for load position (5-8)

finite element model is sufficiently accurate for simulations of occurring steel and concrete stresses for various load situations.

3.2 Most adverse load situation

In order to find the most adverse loading conditions, a finite element analysis (FEA) was carried out with the verified bridge deck model, subjected to two wheel loads (400mm x 400 mm) of 150 kN (LM1), which were varied over seven different locations above the middle longitudinal concrete rib, including the position used for the experimental ultimate failure load test. It was seen that the highest shear stress in the concrete rib network (7.10 N/mm²) occurs for application of the wheelloads between positions (2-8)/(6-8) and (3-8)/(7-8), while for the load situation of the static failure test, a maximum shear stress of only 4.87 N/mm² was found in this numerical simulation.

As a result, the ultimate failure load in ULS, found in section 2.3, was corrected to 325 kN based on these results. It is seen that this load is 8.3 % higher than the prescribed traffic load from EN 1991-2. Thus, it can be concluded that the proposed lightweight steel-concrete bridge deck concept possesses the necessary static resistance to bridge loads. Nevertheless, it should be noted that, in this research, there is only a small margin left for optimization of the bridge deck concept. However, this limitation is related to the applied concrete mixture (REFOR-tec[®] GF5 ST-HS) and, thus, can be reduced by using a product with a higher (tensile) strength.

3.3 Parametric study

In this section of the numerical research, the dimensions of the steel-concrete sandwich deck concept are optimized. As already mentioned, the ultimate load capacity in ULS, based on the concrete shear stress, is only 8.3 % higher than the prescribed traffic load. Consequently, it was found that it is not possible in this research to optimize

the rib dimensions (e.g. rib thickness and/or rib spacing) without increasing the filling degree and deck weight. Hence, only the optimization of the top and bottom steel plate is discussed. In order to do so, five models (with various plate thicknesses) were made, on which the LM1-load (300 kN with identical configuration as given in Fig. 3b) was applied on four different locations, in order to find the maximum occurring stresses.

Ultimate limit state For the evaluation in ULS, the von Mises stress σ_v was assessed. The maximum values can be found in Table 4. Based on the yield strength and the relevant safety factors, the maximum allowable σ_v -value is 158.3 N/mm². From Table 4, it can be seen that when the thickness of the upper steel plate is reduced to 8 mm, this maximum value is exceeded. Though, this limit can easily be increased when steel plates with a yield strength of 355 N/mm² are applied, resulting in an upper limit of 239.1 N/mm². The use of steel with a higher strength grade does imply a slightly increased production cost, but this disadvantage is largely compensated by the weight reduction of the steel-concrete deck, when the thickness of one or both steel plates can be reduced. It can thus be concluded that the ultimate limit state is not the determining situation in the optimization process of the steel plates.

Table 4 Maximum von Mises stresses σ_v [N/mm²]

Thickness t top steel plate	Thickness t bottom steel plate	σ_v top steel plate	σ_v bottom steel plate
10	6	115.1	69.7
8	6	191.8	72.5
12	6	85.3	68.6
10	5	115.9	81.2
10	8	113.9	54.4

Fatigue limit state – General approach For the verification in fatigue limit state (FLS), following assumptions are made:

- Fatigue Load Model 1 (FLM1) from EN 1991-2 is used to assess the maximum stress amplitudes. This load is 70 % of the load from LM1. As a result, the obtained results from the FEAs with LM1 can be used for this FLS approach, when all values are multiplied by 0.7;
- The fatigue assessment is carried out using the damage tolerant method with low consequence of failure. Thus, a partial safety factor for fatigue strength of 1.00 is taken;
- In bridge constructions, various deck panels are interconnected and, additionally, can be connected to the main load carrying system. As a result, several welded joints are required, influencing the fatigue resistance. Fig. 22 summarizes the chosen details and detail categories ($\Delta\sigma_c$) according to EN 1993-1-9 (EN 1993-1-9);
- For a given constant amplitude fatigue limit $\Delta\sigma_c$ a construction detail can endure an unlimited number of cycles when the stress amplitude $\Delta\sigma$ corresponds to:

$$\Delta\sigma \leq 0.7368 \Delta\sigma_c \quad (1)$$

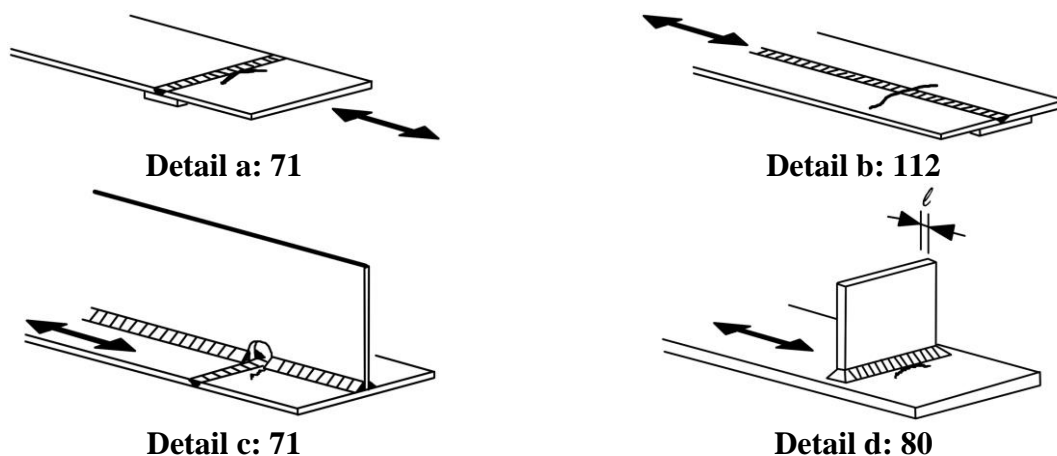


Fig. 22 Details for connections between successive deck panels (a and b) and details for connection between bottom steel plate and supporting crossbeam (c and d)

Fatigue limit state – Transverse stresses The most adverse detail with respect to the transverse stress is detail a. Hence, this stress (for LM1) has to meet the requirement $\Delta\sigma \leq (0.7368 \times 71)/0.7 \leq 75 \text{ N/mm}^2$. The maximum values obtained from the FEAs are listed in Table 5. Since the transverse occurs locally, the minimum value is assumed to be 0 N/mm^2 . In addition, the transverse stresses in top and bottom steel plate are plotted for the original concept ($t_{\text{top}} = 10 \text{ mm}$ and $t_{\text{bottom}} = 6 \text{ mm}$) in Fig. 23 and Fig. 24.

Table 5 Maximum transverse stress (LM1) (compr. = „-„ and tens. = ‘+’) [N/mm²]

Thickness t top steel plate	Thickness t bottom steel plate	σ_{trans} top steel plate	σ_{trans} bottom steel plate
10	6	-62.6	20.2
8	6	-105.9	20.9
12	6	-42	19.4
10	5	-63.1	-25.8
10	8	-61.8	17.2

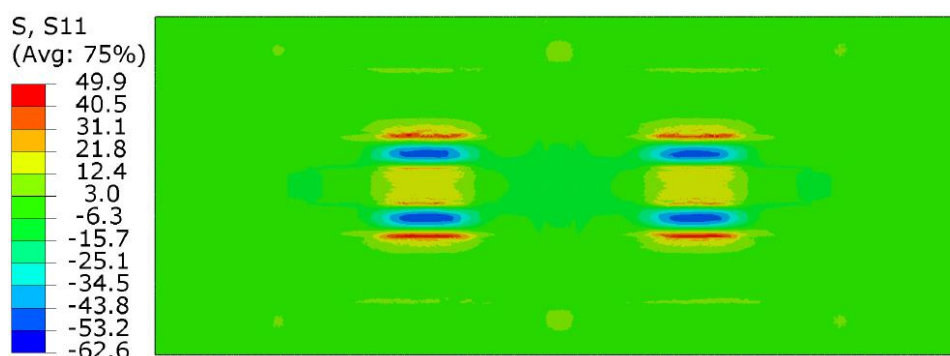


Fig. 23 Transverse stress (LM1) in top steel plate ($t_{\text{top}}=10 \text{ mm}$ and $t_{\text{bottom}} = 6 \text{ mm}$) [N/mm²]

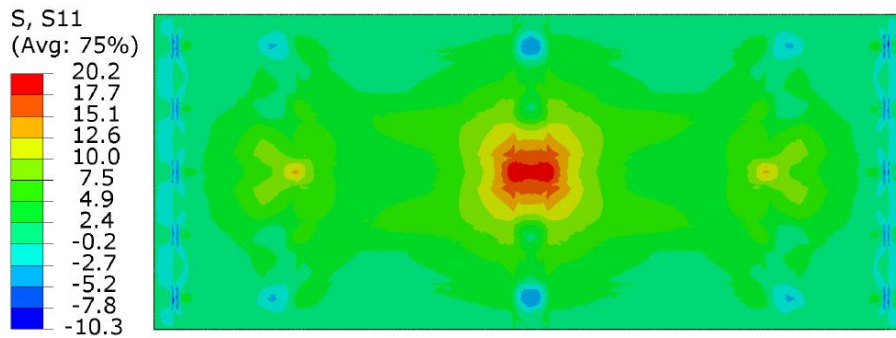


Fig. 24 Transverse stress (LM1) in bottom steel plate ($t_{top}=10$ mm and $t_{bottom} = 6$ mm) [N/mm²]

From Table 5 it is clear that when the thickness of the top steel plate is reduced to 8 mm, the transverse stresses exceed the limit value. In order to estimate the maximum stress for a top plate thickness of 9 mm, the results from Table 5 were plotted as a function of $1/t^2$ (see Fig. 25). Based on the best fitting curve, a value of -80.7 N/mm² was estimated. Hence, the upper steel plate cannot be reduced.

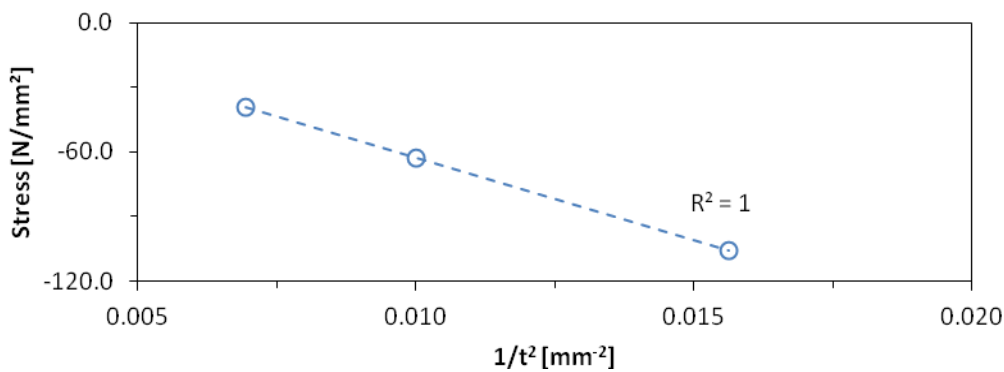


Fig. 25 Numerical transverse compressive stresses for $t_{top}= 8, 10,$ and 12 (LM1)

For the lower steel plate, no problems are expected, since the occurring transverse stresses are relatively small for all models. This plate can thus be reduced to 4/5 mm without problems. Although this plate thickness can be further decreased based on the FLS requirement, a minimum thickness of 4/5 mm is usually applied in the bridge engineering sector.

Fatigue limit state - Longitudinal stresses In contrast with the transverse stresses, the longitudinal stresses are not only influenced by the local behaviour of the deck, but also by its general behaviour. In order to take into account the influence of wheel loads applied in adjacent spans, additional FEMs were made, representing a continuous bridge deck with three spans and supported by 4 rigid supports (Fig. 26). The maximum values (compression in top steel plate and tension in bottom steel plate) are assessed by applying the wheel loads in the centre span. The minimum values (tension in the top steel plate and compression in bottom steel plate) are determined with the wheel loads in the outer span. The resulting maximum values and stress amplitudes are given in Table 6 and Table 7, for top and bottom steel plate respectively.

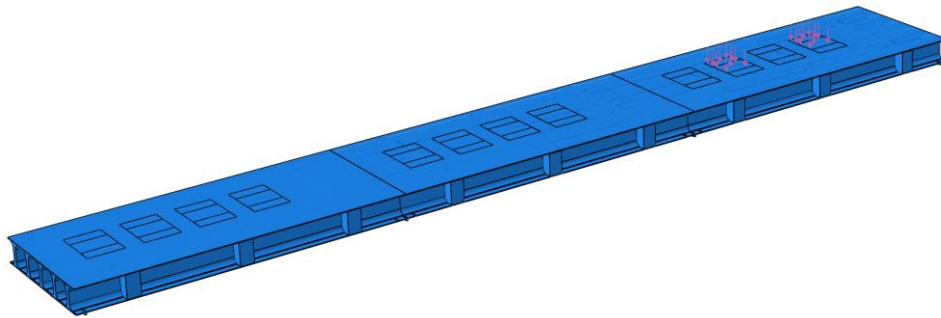


Fig. 26 Continuous bridge deck model

Table 6 Longitudinal stress amplitudes in top steel plate [N/mm²]

Model	$\sigma_{long,max}$	$\sigma_{long,min}$	$\Delta\sigma_{long}$
10-300-50-6	-64.8	10.2	75.0
8-300-50-6	-70.7	11.8	82.5
12-300-50-6	-56.2	9.1	65.3
10-300-50-5	-65.6	10.5	76.1
10-300-50-8	-64.2	9.9	74.1

Table 7 Longitudinal stress amplitudes in bottom steel plate [N/mm²]

Model	$\sigma_{long,max}$	$\sigma_{long,min}$	$\Delta\sigma_{long}$
10-300-50-6	53.9	-12.4	66.3
8-300-50-6	55.0	-12.5	67.5
12-300-50-6	52.9	-12.2	65.1
10-300-50-5	61.3	-14.2	75.5
10-300-50-8	43.2	-9.9	53.1

Also here, detail a from Fig. 22 is the most adverse construction detail with respect to fatigue, resulting in $\Delta\sigma \leq (0.7368 \times 71)/0.7 \leq 75 \text{ N/mm}^2$. For the upper steel plate, it is observed that this value is already obtained for a thickness of 10 mm. The use of a thinner top steel plate is also here not possible. Concerning the bottom steel plate, a $\Delta\sigma$ of 75.5 N/mm² is found for a thickness t of 5 mm, slightly exceeding the maximum allowable stress amplitude. However, it is clear that the position of the transverse weld can be moved in longitudinal direction. It stands to reason that, in this way, a slightly more advantageous position can be found so that $\Delta\sigma \leq 75 \text{ N/mm}^2$ for a bottom steel plate of 5 mm. As a result, it can be concluded that based on the longitudinal stresses, a reduction of the thickness of this plate from 6 to 5 mm is possible.

Fatigue limit state – Connection bottom steel plate and cross girder In order to evaluate this detail, the results from the continuous bridge deck models are used. These results indicate that in the vicinity of the supports rather small transverse stresses are occur, with a maximum of -25.8 N/mm² for the model with a 5 mm thick bottom steel plate. Hence, no problems are expected for this construction detail (detail c in Fig. 22).

For the evaluation of the longitudinal stresses, the maximum value is determined and plotted along a short path in the vicinity of the support (see Fig. 27 and Fig. 28). A stress peak is observed at a distance t . Since this high stress occurs close to the support, it can also be explained by a so-called „notch-effect’ in the vicinity of the support, as this is the case for welded details (Radaj 2006, Niemi 2006, and Eriksson 2003). However, in contrast with the peak stress for welded details, it is seen that here, the stress peak does not occur at the tip of the support. Nevertheless, in this approach the structural hot spot stress method (Niemi 2006) is used to estimate the maximum longitudinal stress at the support, keeping in mind that a different definition of the extrapolation points is needed due to the different location of the maximum peak stress. Based on Fig. 28, it was decided to use the numerical results at a distance $2t$ and $3t$ to determine the hot spot stress σ_{hs} at the notch. The value σ_{hs} for all models is listed in Table 8. Additionally, the hot spot stress for a bottom steel plate of 4 mm is assessed based on these results and also added to this table.

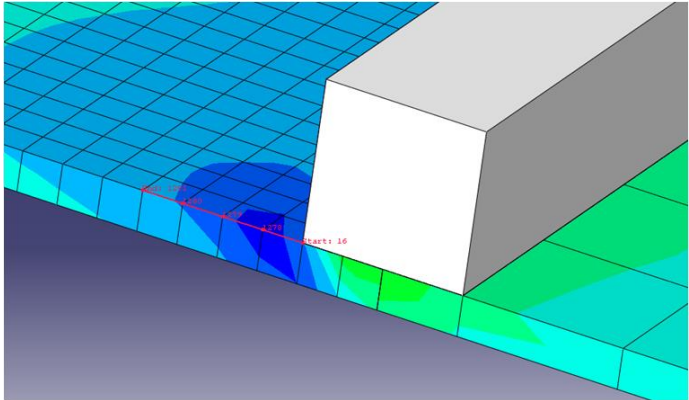


Fig. 27 Detail of longitudinal stress in bottom steel plate ($t = 5 \text{ mm}$)

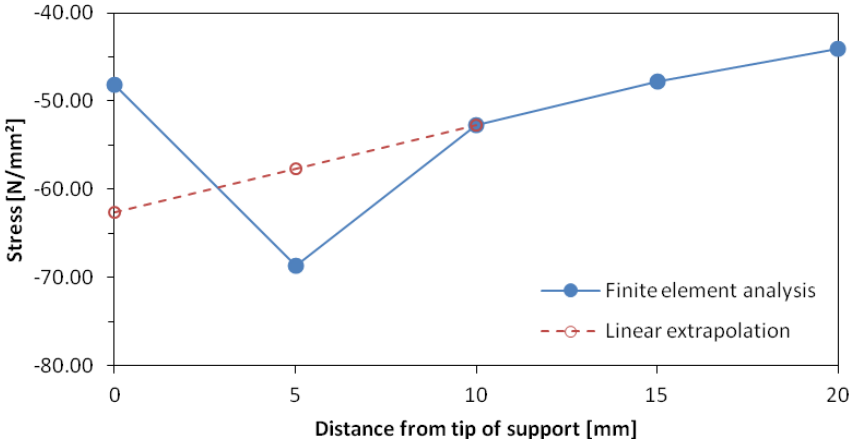


Fig. 28 Surface stress extrapolation in vicinity of support ($t_{\text{bottom}} = 5 \text{ mm}$)

The detail category 80 (detail d in Fig. 22) results in $\Delta\sigma \leq (0.7368 \times 71)/0.7 \leq 84 \text{ N/mm}^2$. From Table 8, it is noticed that the estimated hot spot stress for a bottom

Table 8 Hot spot stresses in bottom steel plate at tip of support [N/mm²]

Thickness t top steel plate	Thickness t bottom steel plate	σ_{hs}
10	6	-54.5
8	6	-55.9
12	6	-53.4
10	5	-62.7
10	8	-40.0
10	4	-70.0

steel plate 4 mm is -70 N/mm² and thus smaller than the limit value. It thus can be concluded that based on this construction detail, the bottom steel plate can be reduced to 4 mm.

CONCLUSIONS

In this paper, the static performance of a new more isotropic lightweight steel-concrete bridge deck concept was investigated. On the one hand, experimental loading tests were carried out to examine its general and local behaviour when concentrated wheel loads are applied on the deck. On the other hand, a numerical study was performed to optimize the bridge deck dimensions. The results of both the experimental and numerical research have led to the following conclusions:

- (a) The 100 kN loading tests showed an identical behaviour of both experimental deck panels. The results pointed out a good spreading of the applied wheel load in transverse direction.
- (b) Based on both the ultimate failure load test and numerical simulations, it can be concluded that the bridge deck concept possesses the necessary static resistance to bridge loads. The maximum bearing capacity in ultimate limit state is determined to be 8.3 % higher than the prescribed traffic load from EN 1991-2. In addition, also the local bending tests on one of the deck panels indicated a sufficient resistance to concentrated wheel loads, with a maximum load capacity in ultimate limit state up to 2.69 times higher than the design load.
- (c) Steel and concrete stresses for numerical models with various plate thicknesses were compared to requirements in both ultimate and fatigue limit state. It was seen that in this research, it is not possible to optimize the rib thickness and/or spacing of the longitudinal beams. For the steel plates, however, it was found that the thickness of the bottom steel plate can be reduced from 6 to 5 mm. For the upper steel plate, the initial thickness (10 mm) cannot be decreased.

ACKNOWLEDGEMENTS

The authors wish to express their gratitude to the Research Fund of the Ghent

University College for financial support and to B. Devriendt, P. Ost, L. Van Boxstael, and K. De Sutter for their assistance in the production of the formworks and test members, the execution of the experiments, and the numerical calculations.

REFERENCES

- Chen, W.-F., Duan, L. (2000), "Bridge Engineering Handbook," Boca Raton (FL): CRC Press LLC
- Connor, R. et al. (2012), "Manual for design, construction, and maintenance of orthotropic steel deck bridges," US Department of Transportation – Federal Highway Administration (FHWA), Washington (DC)
- Cusson, D., Lounis, Z., Daigle, L. (2010), "Benefits of internal curing on service life and life-cycle costs of high-performance concrete bridge decks – A case study," *Cem. Concr. Compos.*, **32**(5), 339-350
- De Corte, W. (2005a), "Fatigue behaviour of steel orthotropic decks subjected to traffic loads (PhD thesis in Dutch)," Ghent University, Ghent
- De Corte, W., Van Bogaert, P., De Backer, H. (2005b), "Efficiency of closed stiffener orthotropic deck panels for railway bridges," *Bridge Struct. – Assessment, Design & Construction*, **1**(3), 203-210
- EFNARC (2005), "The European guidelines for self-compacting concrete – Specification, production and use," The European Federation of Specialist Construction Chemicals and Concrete Systems
- Eriksson et al. (2003), "Weld evaluation using FEM: a guide to fatigue-loaded structures, Industrilitteratur, Stockholm (Sweden)
- Helincks, P. et al. (2013), "Experimental investigation of the influence of the bond conditions on the shear bond strength between steel and self-compacting concrete using push-out tests," *Key Eng. Mater.*, **525-526**, 205-208
- Lombardi, N.J., Liu, J. (2011), "Glass fiber-reinforced polymer/steel hybrid honeycomb sandwich concept for bridge deck applications," *Compos. Struct.* **93**(4), 1275-1283
- Niemi, E., Fricke, W., Maddox, S. (2006), "Fatigue analysis of welded components: designer's guide to the structural hot-spot stress approach," Woodhead
- Nguyen, H.-T., Chu, Q.-T., Kim, S.-E. (2011), "Fatigue analysis of a pre-fabricated orthotropic steel deck for light-weight vehicles," *J. Construct. Res.*, **67**(4), 647-655
- Radaj, D., Sonsino, C., Fricke, W. (2006), "Fatigue assessment of welded joints by local approaches," Woodhead, Cambridge (England)
- Reid J. & Sons Ltd, "REIDsteel – bridging the world since 1919," www.steel-bridges.com
- Sim, H., Uang, C., Sikorsky, C. (2009), "Effects of fabrication procedures on fatigue resistance of welded joints in steel orthotropic decks," *J. Bridge Eng.*, **14**(5), 366-373
- Tecnochem (2007), "Technical datasheet Tecnoepo 400," Tecnochem Italiana S.p.A. , Bergamo (Italy)
- Tecnochem (2010), "Datasheet REFOR-tec® GF5 ST-HS," Tecnochem Italiana S.p.A. , Bergamo (Italy)
- Teixeiras de Freitas, S., Kolstein, H., Bijlaard, F. (2010), "Composite bonded systems for renovations of orthotropic steel bridge decks," *Compos. Struct.*, **92**(4), 853-862